3D T cell motility in jammed microgels

Tapomoy Bhattacharjee[1] and **Thomas E Angelini**[1,2,3]

[1] Mechanical and Aerospace Engineering Department, University of Florida, Gainesville, FL, United States of America
[2] J. Crayton Pruitt Family Department of Biomedical Engineering, University of Florida, Gainesville, FL, United States of America

E-mail: t.e.angelini@ufl.edu

CrossMark

Abstract

Exploration of *in vitro* cell behavior in 3D space has revealed that cell morphology, cell generated forces, and the architecture of the intracellular mechanical machinery differ from their 2D counterparts, demonstrating the importance of investigation in 3D. However, current 3D methods employ continuous polymer networks to study cells in 3D which present numerous challenges associated with the need for transient pore-space to enable cell motion and the complexities of controlling the 3D cell distribution. To overcome these challenges, we have developed a 3D culture medium made from jammed microgels; the rheological properties of jammed microgels swelled in liquid cell growth media allow the dispersal of cells in into a 3D environment with well-defined structural and material properties. In this work, we explore the motility of T cells in systems of jammed microgel growth media prepared with different yield stresses, finding time-scale and length-scale dependent dynamics that are correlated with the pore-space between the microgels. Jammed microgels represent a class of soft matter with unique properties that has not been leveraged for the study of cell motion or mechanics in 3D space; our observations of cell motion through jammed microgels demonstrate how T cells navigate porous environments and provide guidance for a multitude of future investigations in unexplored territory.

Keywords: cell motility, 3D culture, porous media, microgels, T cells

(Some figures may appear in colour only in the online journal)

Introduction

Granular-scale polyelectrolyte microgels can be packed into a jammed state having dominantly solid-like properties when left unperturbed and having dominantly fluid-like properties under sufficiently high applied shear stress [1–5]. These rheological properties make jammed microgels useful in many applications and have motivated numerous detailed investigations, including experiments and theoretical models [5–9], recently connecting rheological properties to single-chain polyelectrolyte physics [10]. Microgels have been used as a major rheological modifier of personal care products for decades [11–16] and more recently jammed microgels have been leveraged as a support material for 3D printing complex structures made from colloids, soft hydrogels, elastomers, and living cells [17–19]. For 3D printing structures made from cells, a jammed system of microgels was swelled in liquid cell growth media, where it

was found that the support material could serve as a 3D growth medium in addition to performing as a support for 3D printing; cells were found to migrate and proliferate in the jammed microgel medium [20]. 3D cell behavior has been explored using biopolymer networks and templated scaffolds [4, 21], yet numerous challenges remain that are associated with controlling 3D cell distribution and with the transience of networks as they form and degrade. By contrast, jammed granular growth medium represents a nearly unexplored tool for dispersing cells into a rheologically well-defined 3D environment for broad experimentation; cells are easily dispersed in jammed microgel growth media having a pre-defined elastic modulus and yield stress. Thus, investigations of cell behavior within jammed materials will introduce an entire class of soft matter to cellular biophysics research that may uncover cell behaviors that only occur within materials having the unique rheological properties of jammed granular matter.

Here we explore T cell motion in systems of jammed microgel growth media prepared at various yield stresses. By

[3] Author to whom any correspondence should be addressed.

dispersing fluorescently labeled T cells in jammed microgel growth media and imaging with time-lapse confocal fluorescence microscopy, we track individual cells in 3D and characterize their behavior. Analysis of cell step-size distributions reveals a relationship between qualitative cell motility and microgel yield-stress; with increasing microgel yield stress, cell migration changes systematically from super-diffusive to diffusive to sub-diffusive. More detailed analysis of the mean-squared displacements (MSD) demonstrates the same general trend at short time-scales, yet shows the opposing trend at the longest time-scales. This complex behavior is found to be coupled to the porosity of packed microgels; empirical observations show that the T cells move without causing any major microgel rearrangements, which suggests that cells move through pre-defined 3D pore-space in the jammed microgel. Measurements of pore-space between microgels uncover a relationship between pore-size and cell motion; at short time-scales, the cell step-size is approximately the pore-size. By estimating the most probable time required for an average sized cell nucleus to pass through a small pore, we find that the cells move faster through smaller pores, as has been observed in T cells passing through small constrictions. While the investigations described here are on individual cells, they represent the groundwork necessary for future investigations of collective motion in jammed microgel culture media.

Results and discussion

Jammed microgels as 3D cell culture medium

To enable investigations of 3D cell behavior within jammed microgels, we formulate a 3D culture medium made with packed microgels and perform rheological measurements on samples without cells using a roughened cone-plate geometry on a rheometer. Jammed microgel growth medium is prepared by dispersing a commercially available microgel, Carbomer 980, directly into liquid cell growth medium at three different polymer concentrations: 0.72 wt%, 0.60 wt% and 0.50 wt% (see Methods). To ensure the microgel medium is compatible with cell culture conditions, we set its pH to 7.4 under the standard incubation conditions of 5% atmospheric CO_2 and 37 C. To measure the shear moduli of the jammed microgel media, we perform frequency sweep tests under incubation conditions, applying a small oscillatory strain of 1%. For all three formulations, we find that the elastic shear moduli are relatively independent of frequency and larger than the viscous shear moduli; this rheological behavior indicates that when subjected to small perturbations, jammed microgel culture media is dominantly solid-like (figure 1(c)). When subjected to unidirectional shear at high rates, the shear stress follows a power law dependence on the shear-rate and becomes independent of shear-rate below a certain crossover shear-rate. The shear-rate independent shear stress equals the yield stress (σ_y) of the 3D growth medium and is obtained by fitting the unidirectional shear test data to the Herschel–Bulkley model, $\sigma = \sigma_y(1 + (\dot{\gamma}/\dot{\gamma}_c)^n)$, where σ is the measured shear stress, $\dot{\gamma}$ is the applied shear-rate, $\dot{\gamma}_c$ is the crossover shear-rate, and n is a constant of order 0.5. We find that the samples prepared at
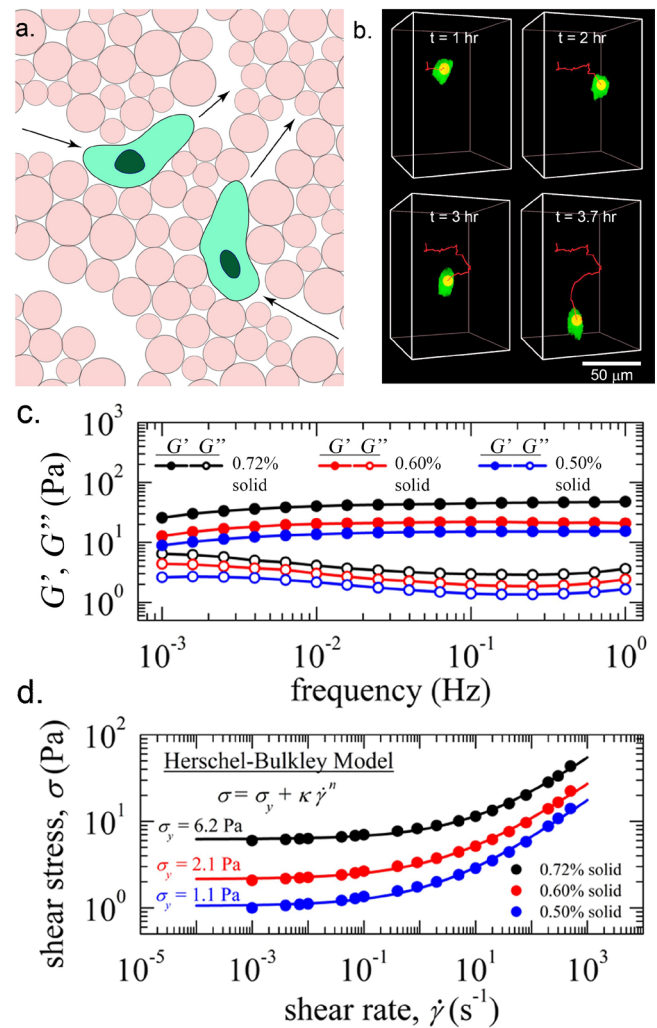
Figure 1. T cells in jammed microgel cell growth media.
(a) Systems of jammed microgels swelled in liquid cell growth medium are used as 3D cell culture media which can support motile cells. (b) 3D motion of cytotoxic mouse T cells (CTLL-2, ATCC) are monitored inside a jammed microgel growth medium using confocal fluorescence microscopy and 3D cell tracking software.
(c) A frequency sweep test at 1% applied strain is performed, finding that the elastic moduli are higher than the viscous shear moduli. This rheological property indicates that the jammed microgel growth media used in these studies are dominantly solid-like under small applied stresses. (d) When subjected to a unidirectional shear, the jammed microgel growth media fluidize at high shear rates. At low shear rates, shear stresses become independent of shear rate and these plateau stresses are used to determine the yield stress.

0.72 wt%, 0.60 wt% and 0.50 wt% have yield stresses of 6.2 Pa, 2.1 Pa and 1.1 Pa, respectively (figure 1(d)).

The jammed microgel culture medium creates an environment in which, in the absence of added ECM, most tissue cells are not expected to exhibit their generally known functions and behaviors. However, T cells are the most motile cells in an immune responsive organism, travelling from the lymph node to a diversity of different peripheral tissues. During this process, T cells move through environments of widely varying mechanical and chemical properties [22]. Therefore, we choose to investigate the details of T cell motion in this study because among all other cell types typically used for *in vitro* migration and mechanics studies, we expect T cells to

most readily navigate the microenvironment presented by the jammed medium without needing to introduce the additional variable of natural ECM materials. To observe T cell motility in 3D, we grow cytotoxic mouse T cells (CTLL-2, ATCC) in a suspension culture flask. The cells are stained with whole-cell fluorescent dye (Cell Tracker Green, Thermofisher) before dispersing into the jammed granular microgel growth medium by gentle pipette mixing. The dispersed cells are imaged using a controlled environment confocal micro-scope maintained at 37 °C and 5% CO_2. The low polymer concentrations of all three jammed microgel growth media samples allow us to image cells dispersed in 3D without any major attenuation of fluorescence intensity. We find that the T cells can move freely inside the jammed microgel growth medium over the course of imaging which lasts for approximately 24 h. Previous viability tests of these T cells in jammed microgel growth media reported no apparent cell death over the course of 24 h [20]. It is intriguing that T cell motility is observed in jammed microgel growth medium without any added extracellular matrix (ECM), which is potentially related to T cells' ability to migrate through the diversity of environments throughout the body [22]. We find that these T cells move faster than the epithelial cells reported previously [20]. Thus, we choose the delay time between collecting fluorescence z-stacks to be 5 min, which is frequent enough that cells do not move by more than their own diameter between measurements and infrequent enough to eliminate photo-bleaching and detectable cell death from potential photodamage. We analyze the time series using custom written scripts in MATLAB for stack segmenta-tion, cell identification, and tracking in 3D. The geometric center of each cell is used to measure its position at every time frame. To perform statistical averages on individual cell tracks as well as the entire ensemble, we impose a minimum track length requirement of 2.5 h. With this restriction we are still able to perform measurements on the majority of cells in the imaged sample volume (approximately $N = 90$–200 cells per sample and three different replicate samples). We tested for stationarity over this time interval by checking the time-dependence of the ensemble averaged step-size at the min-imum delay time. We found no significant drift in this meas-urement over time, consistent with stationary behavior.

Categorizing T cell motion with step size distributions

To broadly classify T cell motion in granular culture media and explore how different yield stresses affect these motions, we calculate the distance traversed by each cell with increasing lag-time, given by $r(\tau) = |\mathbf{r}(t + \tau) - \mathbf{r}(t)|$, where $\mathbf{r}(t)$ is the position vector of a cell at time t and τ is the lag-time between measurements. For each lag-time τ, the step-size distribution, $p(r)$, is computed, which is a piecewise constant probability density function measured across all cells and all experimental times, t. In the three formulations of jammed microgel media tested here, we find that $p(r)$ at each τ have similar shapes but shift towards higher step sizes with increased τ. This is generally how step size distributions evolve for translocating
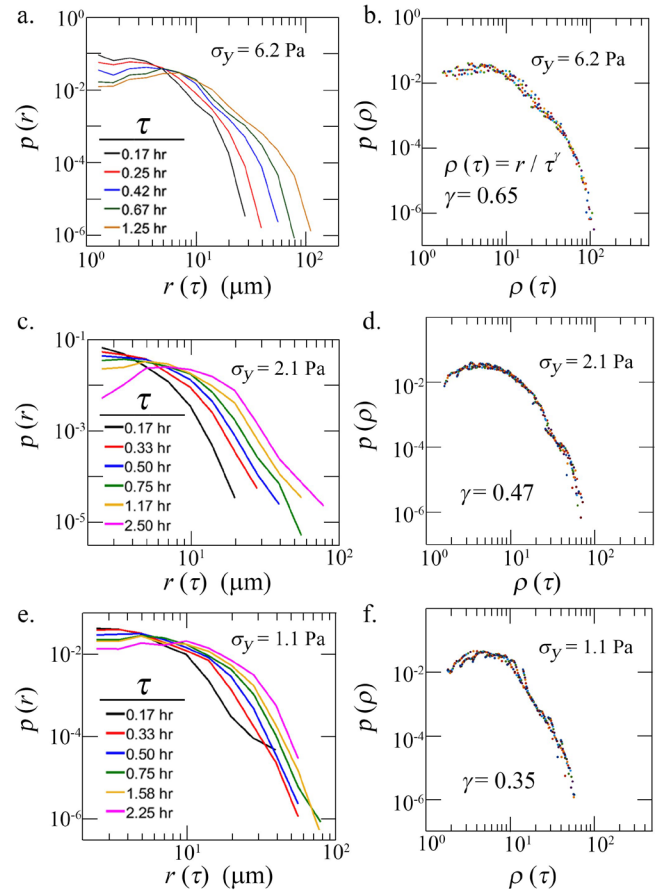
Figure 2. Step size distribution. (a), (c) and (e) The distances travelled by all the cells over different time-scales are captured by a family of step size distributions, which are the piecewise constant probability density functions of cell displacements at each measured time difference, averaged over all cells. (b), (d) and (f) By re-scaling the step-sizes by their corresponding delay times, τ, raised to the power γ, the step size distributions at different τ collapse onto single curves. We find that the cell motility in 6.2 Pa microgel medium is consistent with super-diffusive motion ($\gamma > 0.5$); cell motility in the 2.2 Pa yield-stress medium appears diffusive ($\gamma \approx 0.5$); cell migration in the 1 Pa yield-stress medium produces appears sub-diffusive ($\gamma < 0.5$).

objects. To test whether there is any universal trend in these distributions with increasing time-delay, we re-scale the step size $r(\tau)$ by τ^γ, yielding a normalized step-size distribution function $p(\rho)$, where $\rho(\tau) = r(\tau)/\tau^\gamma$ [23]. One can think of γ as a variable that indicates different classes of motion. Super-diffusive motion corresponds to $\gamma > 0.5$; sub-diffusive motion corresponds to $\gamma < 0.5$; diffusive motion corresponds to $\gamma = 0.5$. We find that the step size distribution of cells in jammed microgels of highest yield stress, 6.2 Pa, can be col-lapsed onto a single curve by choosing a $\gamma = 0.63$ (figure 2(b)). Similarly, the step size distributions of cells in jammed microgels of 2.2 Pa and 1.1 Pa yield stresses collapse with $\gamma = 0.47$ and $\gamma = 0.35$ respectively (figures 2(d) and (c)). Thus, this analysis suggests that cell motility in jammed microgels having intermediate yield-stress is almost diffu-sive; at higher yield stresses, cell motion appears to be super-diffusive; at lower yield stresses, cell motion appears to be sub-diffusive (figure 2). While it is tempting to conclude that
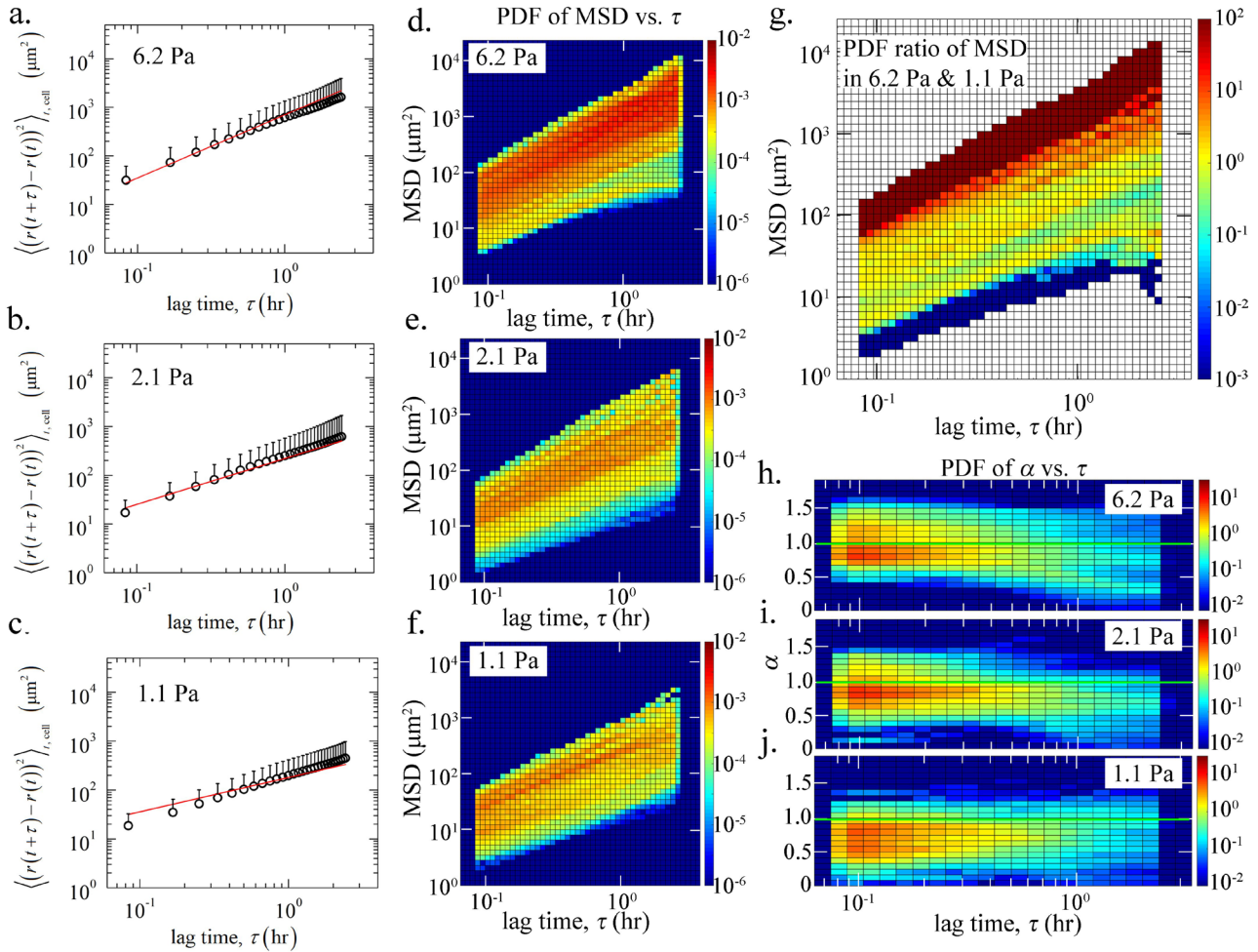
Figure 3. Mean squared displacement analysis. (a)–(c) Ensemble averaged mean squared displacements (open circles) are well described by single power laws, given by $\mathrm{MSD}\,(\tau) = K\tau^{2\gamma}$ (red lines), where γ is the power found in step-size distribution analysis. Errorbars denote one standard deviation above each mean. (d)–(f) 2D piecewise constant probability density functions of single-cell MSDs, and lag times, τ, show the overall increasing displacement with time; examining the most probable motions and the edges of the distrubtions indicate a general speeding-up of cells with increasing microgel yield-stress. (g) The ratio of the PDFs shown in (d) and (f) illustrate this general trend. (h)–(j) We treat each MSD as a power law having a τ dependent exponent, given by $\mathrm{MSD}\,(\tau) = K\tau^{\alpha(\tau)}$ and plot the 2D PDF of α and τ. In the highest yield stress culture medium (6.2 Pa), we find the strongest transition between large α and low α with increasing time; this transtion is weakened in the intermediate material (2.1 Pa); the trend appears to weakly reverse in the lowest yield stress material (1.1 Pa). The green line at $\alpha = 1$ indicates the diffusive threshold.

this analysis accurately characterizes T cell motion within these different media, cell populations are very heterogeneous in terms of motion, so analysis that accounts for cell-to-cell variations may lead to different conclusions.

Population heterogeneities reveal transitions between classes of motion

While the collapse of $p(r)$ across lag-times allows the broad characterization of cell motion in different microgel environments, analyzing individual cell motion as a function of lag-time can elucidate more detailed dynamics. To perform such analysis, we employ a standard tool for qualitatively classifying and analyzing the motion of large collections of individual objects: the mean-squared displacement (see Methods). From each measured cell track we calculate the mean squared displacement as a function of lag time, given by

$\mathrm{MSD}(\tau) = \left\langle (\mathbf{r}(t + \tau) - \mathbf{r}(t))^2 \right\rangle$, where angle brackets indicate an average over all experimental time points, t. The ideal cases are captured by a simple power law behavior, given by

$$\mathrm{MSD}(\tau) = K\tau^{\alpha},$$

where $\alpha = 1$ represents diffusive motion, $\alpha > 1$ represents super-diffusive behavior, $\alpha < 1$ indicates sub-diffusive motion, and K is a transport coefficient. We find that the ensemble average over single cell MSDs is well described by a single power law, as would be expected from the step-size distribution analysis above, where $\alpha = 2\gamma$ (figures 3(a)–(c)). However, for cells in microgel media at any of the yield stresses tested, we find the single-cell MSDs are not simple power laws; by contrast, α varies with τ and the MSDs vary in shape and overall scale between different cells, demonstrating that the system is non-ergodic. To illustrate the variability in MSDs and their overall shapes as a function of τ,

we compute a 2D piecewise constant probability density function, using logarithmically spaced bins in MSD and τ values (see Methods for normalization procedures). Plots of these 2D PDFs show qualitatively that cells move faster in materials with higher yield stress (figures 3(d)–(f)). This trend is well illustrated by plotting the ratio of the highest yield stress PDF to the lowest yield stress PDF; since these PDFs are normalized, this ratio captures the relative probability density of cells moving a given distance over a given time within the two materials (figure 3(g)).

To quantify this complex motion as a function of lag time, we treat each single-cell MSD as a power law having a τ-dependent exponent, given by $\mathrm{MSD}(\tau) = K\tau^{\alpha(\tau)}$. To determine α as a function of lag time we re-sample the MSDs on a logarithmically spaced τ axis and compute the logarithmic derivative of each MSD with respect to τ (see Methods for details). We then count the occurrences of α–τ pairs within bins from all single cell MSDs and create 2D piecewise constant probability density functions where α bins are linearly spaced and τ bins are logarithmically spaced (see Methods for the normalization procedure). The profiles captured in these PDFs demonstrate how cell motion differs among the three different jammed microgel systems. We find that for cells moving inside the jammed microgel system of highest yield stress (6.2 Pa), a large population of cells is super-diffusive at short time-scales ($\alpha > 1$) and sub-diffusive at long time-scales ($\alpha < 1$). The super-diffusive population at short time-scales is reduced in the intermediate yield stress material (2.2 Pa); the sub-diffusive population at the longest time-scales is also reduced. Cells migrating through the lowest yield stress material (1.1 Pa) dominantly exhibit sub-diffusive motion with $\alpha < 1$, though at the longest time-scales the distribution of α rises again and approaches 1. One might expect ballistic motion at very short time-scales; we do not see such motion, possibly limited by the 5 min sampling interval employed here. While the general trend between α and yield stress is generally consistent with that found by analyzing step-size distribution functions (figure 2), the 2D PDF analysis reveals details about τ-dependent motion that appears to be washed out by the previous analysis. For example, cells appear to be increasingly 'trapped' at long time-scales with increasing yield-stress; the opposite trend occurs at the shortest time-scales. These opposing behaviors suggest that within the different jammed culture media, environmental factors other than yield-stress alone may contribute to cell motion. We explore these other potential factors below.

Cell-microgel interactions

Cell generated stresses in 3D are often studied by dispersing cells in biopolymer matrix and monitoring matrix deformation in 3D. In such experiments, cells attach to fibers and contract to deform the matrix [24, 25]. By contrast, in a jammed microgel medium the cells likely do not form specific adhesions to the microgel polymer strands; T cells are known to 'swim' through adhesion free environments using a type of amoeboid motility [26]. The correlation between cell motion and the yield stress of microgel culture media, described

above, suggests that cells may be locally yielding the packed microgels as they migrate. To estimate the level of stress potentially generated as cells move, we employ the Herschel–Bulkley model that describes the relationship between stress within the jammed microgel medium and shear rate, given by $\sigma = \sigma_y 1 + (\dot{\gamma}/\dot{\gamma}_c)^n$, as previously discussed. We estimate the local shear-rate, $\dot{\gamma}$, from the cell speed, v_{cell}, and the characteristic cell size, l_{cell}, approximately given by

$$\dot{\gamma} \approx \frac{v_{cell}}{l_{cell}}.$$

To determine an average value for v_{cell}, we compute the root-mean-square speed from the mean-square displacements, given by $v_{rms}(\tau) = \sqrt{\mathrm{MSD}(\tau)}/\tau$. The fastest cell speeds found in this manner are approximately 160 μm h^{-1}. Approximating the typical cell length-scale to be 20 μm, this produces a stress less than 3.5% larger than the lowest yield stress of jammed media explored here. This back-of-the-envelope analysis therefore predicts that as cells move through the jammed media, they may not be driving substantial rearrangements of the microgel granules.

Guided by this prediction, we perform experiments to observe how moving cells deform the jammed microgels that constitute their microenvironments. We disperse a mixture of cells and 10 μm diameter fluorescent beads inside jammed microgel media and image their motion over time using a confocal microscope. We identify each cell and fluorescent bead at every time frame and track their motions over time. Qualitative analysis of these time lapse images reveals that cell motility inside the jammed microgel media does not induce any visible bead motion, yet the cells move through long, tortuous paths (figure 4(a)). To quantitatively measure the cell induced motion of beads, we measure the displacement of the fluorescent beads as function of cell-bead distance for every cell-bead pair at every instant in time, averaging over the ensemble of cell-bead pairs. We find that, irrespective of the distance between a moving cell and a microbead, the average displacement of the fluorescent beads about their mean position is within the order of 1 pixel size (1.24 μm) in our images (figure 4(b)). Within the range of stress cells are capable of generating, typically the kPa range, microgels are essentially incompressible, having a bulk modulus in the MPa range [27]. Thus, if the microgels formed a tightly packed continuum they would have to flow in response to nearby moving cells within a hydrodynamic radius of at least 20 μm, with an overall fluctuation in position of about the same length-scale. The lack of detectable bead motion for all measured cell-bead distances indicates that the moving cells find paths inside the jammed microgels that do not require yielding or major structural particle rearrangement as they migrate. Moreover, this observation indicates that the microgel systems are not appreciably aging throughout the experiments.

Correlation between cell motion and pore size distribution

To further investigate the paths that migrating cells follow within jammed microgel media, we use a solution of long chain fluorescent dextran and allow it to diffuse through three
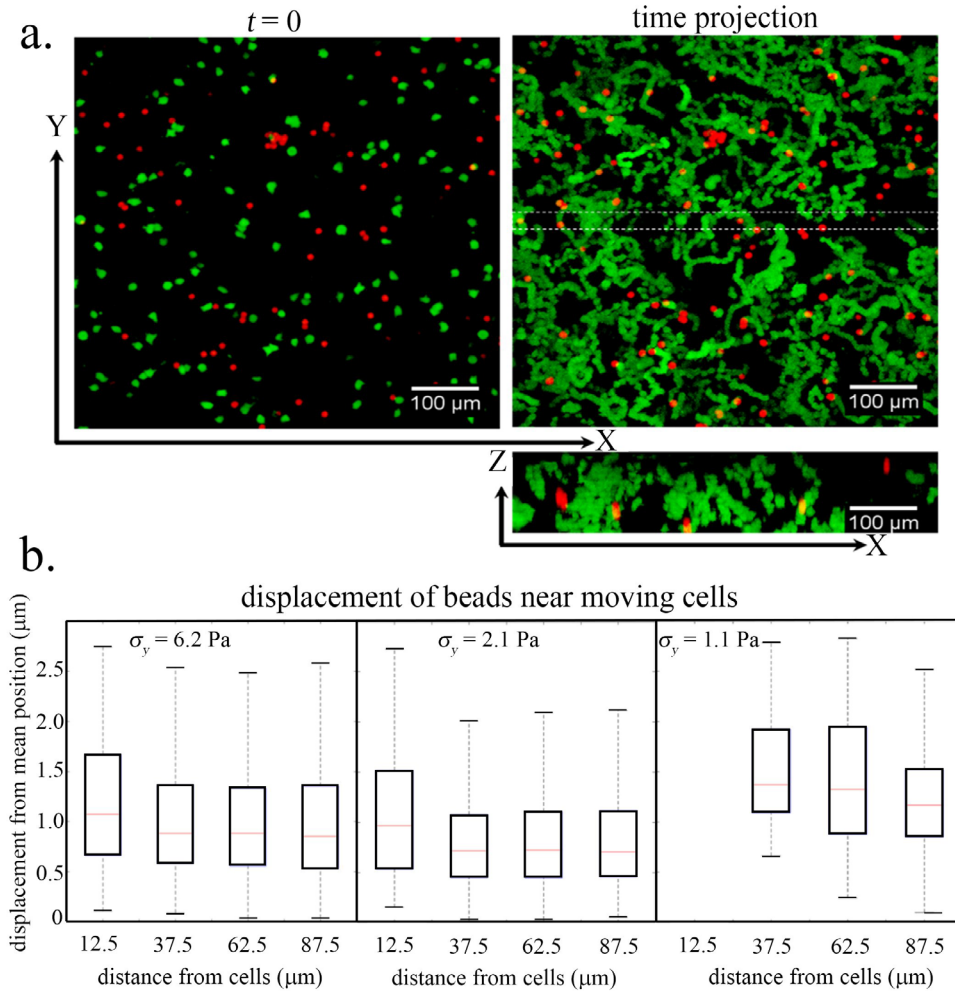
Figure 4. Co-dispersion of cells and fluorescent beads. (a) CTLL-2 T cells stained with CMFDA (green) 10 μm fluorescent beads (red) are dispersed in the jammed microgel medium. Maximum intensity projection of confocal time series along Z axis as well time demonstrates no visual evidence of fluorescent bead movement parallel to the X–Y plane while the T cells move and explore the microenvironment of the beads. Maximum intensity projections along the Y axis and time for a smaller section of the data also shows minimal motion of the microbeads. The small amount of smearing along the z axis is associated with the elongated point-spread function in that direction. (b) The average 3D displacements of the fluorescent microbeads from their mean positions are measured as a function of their distance from nearest cell at every time point. The average motion of beads is found to be approximately of the order of one pixel size.

different microgel systems. A small volume (10 μl) of concentrated fluorescent dextran solution in PBS is placed in a glass bottom petri dish and 4 ml of jammed microgel samples is gently deposited on top of the dextran layer, filling the entire width of the dish. We wait for 1 h for the fluorescent dextran to diffuse into the pore-space throughout the microgel. High resolution confocal images are then acquired to find the 3D spatial distribution of dextran. We use these high-resolution fluorescence images to calculate a spatial auto-correlation function of fluorescence intensity. The length-scale at which the correlation function reduces to half its maximum value is chosen to determine a correlation length, which we use as the average measure of pore size between microgels. As expected, we find that with increasing microgel concentration, this average pore size decreases; the jammed microgel system with 6.2 Pa yield stress has the smallest pore size of approximately 0.75 μm, while the 1.1 Pa yield stress system has largest pore size of approximately 1.1 μm (figures 5(b) and (c)). These pore sizes are consistent with the expected

range for packed spheres of diameter between 3.75 μm and 5.5 μm; this size-scale is consistent with the order of magnitude expected for lightly packed carbomer microgels.

While this approach to pore size measurement may capture the average pore size, the shape of the dextran fluorescence correlation function indicates a broad distribution of pore sizes, consistent with the large degree of polydispersity of microgel size previously found [10]. Thus, we hypothesize that T cells may be using the full distribution of pore space to migrate—in particular, the larger pores. To determine a measure of pore size distribution in the jammed microgel media, we use Otsu's method [28] to threshold the high-resolution fluorescence images of dextran permeated microgel media, and compute a distance transform. Each pixel value in the distance transform map represents the average distance between a dextran-rich location and all the nearby dextran-depleted locations; we double the values in the distance transforms so that a pixel located in the center of a pore reports the average pore diameter. This approach was previously employed to measure the

J. Phys. D: Appl. Phys. **52** (2019) 024006

T Bhattacharjee and T E Angelini
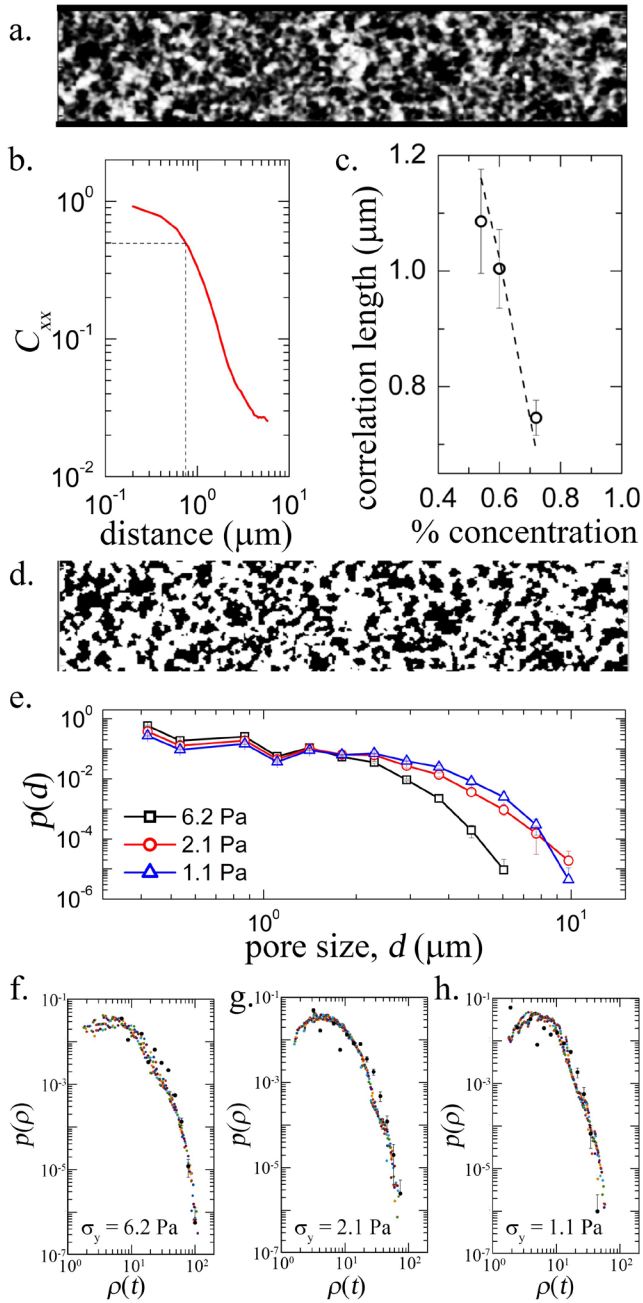
Figure 5. Pore sizes in microgel media. (a) Long chain fluorescent dextran is allowed to diffuse through three different microgel systems and single planes of these samples are imaged using a confocal microscope. (b) The spatial auto-correlation function of the fluorescence images are computed to measure correlation lengths (dashed lines mark the full-width-half-max, which we use as the correlation length). (c) We estimate the pore size from the full-width-half-max, which decreases with increasing microgel concentration. (d) The fluoresence images are thresholded and distance transformed to compute a pore-size distribution function. (e) The pore-size distribution functions show that the percentage of larger pore space increases with decreasing microgel yield stress. (f)–(h) We re-scale the pore-size distribution following the procedure used for step size distribution, finding a collapse of pore-size distribution onto the cell step-size distributions.

mesh-size of collagen networks [29]. Calculating a piecewise constant probability density function of these distance values, d, produces a length-scale sensitive distribution of available space through which cells can migrate, $p(d)$ (figure 5(e)). We

note that these pore size distributions appear to have the same shapes as the step-size distributions found for cells migrating through the different formulations of jammed microgel media (figure 2). Indeed, by computing re-scaled pore-sizes, $\rho = d/\tau^\gamma$ and creating a normalized pore-size distribution function, $p(\rho)$, we find that the pore-size distribution functions collapse onto the step-size distribution functions using $\tau = 0.8$ min and the corresponding γ previously measured for each of the three different jammed microgel samples (figures 5(e)–(g)). Since our sampling interval is 5 min, this collapse of distributions for $\tau = 0.8$ min represents an extrapolation of long-time observed behavior to short-time behavior that is not measured in our experiments. This extrapolation could be verified if step-sizes were measured at $\tau = 0.8$ min intervals, and the resulting distribution collapsed onto all the long-time distributions. Our results show that this step-size distribution would also lay on top of the pore-size distribution without any re-scaling, indicating that cells opportunistically use the available pore space around them to make instantaneous moves. Micron-scale motions over time-scales of about a minute are most likely associated with local cellular shape changes that ultimately result in longer time-scale translocation, such as the extension of filopodial protrusions. Further experimentation is required to determine whether $\tau = 0.8$ min is a characteristic timescale associated with T cell motion the three microgel systems tested here.

These measurements of the 3D pore space within the jammed microgel media create the opportunity to study T cell migration through constrictions. Similar to trans-endothelial migration, as a T cell moves through small channels and pores *in vitro*, the nucleus is one of the determining factors of migration speed [30]; cells move faster through smaller pores down to a cut-off length-scale at which nuclear damage occurs [31]. To examine whether the same principle may apply to T cell migration through jammed microgel media, we estimate the most probable re-scaled step size from the approximate peak location in the collapsed distribution functions shown in figures 2(b), (d) and (f), which we write as $\rho_{nuc} = d_{nuc}/\tau_{nuc}^\gamma$, where d_{nuc} is the nucleus diameter and τ_{nuc} is the characteristic time-scale for a cell to take a step of length d_{nuc}. We consider an average nucleus diameter to be 5 μm, about 1/4th of the average 20 μm cell size. From the most probable re-scaled step size, we calculate τ_{nuc}; we find $\tau_{nuc} = 0.85$ h for 6.2 Pa media, $\tau_{nuc} = 1.45$ h for 2.1 Pa media, and $\tau_{nuc} = 1.9$ h for 1.1 Pa media. Identifying the step-size distribution with the pore-size distribution, guided by the analysis above, we infer that in 3D jammed microgel environments with smaller pores, cells move their nuclei at higher speeds as they translocate constrictions. This finding is consistent with the observation of cell motion through different sized constrictions, though direct observations of cell motion within pores of known size are required to confirm the direct relationship between cell speed and constriction size.

Conclusion

Jammed microgels represent an entire class of soft matter that can be used to support cells in 3D but that has been practically

J. Phys. D: Appl. Phys. **52** (2019) 024006

T Bhattacharjee and T E Angelini

unexploited in this area, whether for fundamental investigations or technological applications. The results described here have just scratched the surface of potential research areas, from 3D cell mechanics measurements, to collective cell behavior. For example, by combining the types of experiments described in this manuscript with the 3D bioprinting approaches recently developed in the same microgel culture medium [17, 20], studies of T cell chemotaxis toward 3D printed tumors can be performed with a high degree of control and versatility. Tumoroids of differing size and cell composition can be 3D printed and T cells can be placed at pre-defined distances from the tumor surface to study the kinetics of cytokine production and diffusion, signaling the T cells to attack the tumor [32]. Control experiments have already shown that small molecules diffuse through the jammed microgel medium as predicted by an experimentally implemented boundary value problem using controlled-release polymer films embedded in the microgel medium [20]. The results described here, showing that T cells migrate through a pre-defined pore-space, will serve to guide interpretation of such future experiments; we previously believed that migrating T cells would yield the microgel medium, creating locally stressed or yielded zones around migrating cells that would result in cell-cell interaction over distances spanning many cell-lengths. Indeed, we performed many analyses on the 3D cell tracks collected for this manuscript that tested for cell-cell interactions. We found no evidence of spatiotemporal correlations between pairs of cells as a function of the distance between them. Performing tests of chemotaxis in dense systems of T cells moving together up a gradient of chemoattractant may produce these effects. Finally, while the jammed microgel culture medium is not intended to be a superior tissue-mimic compared to natural ECM scaffolds, we note that many tissues *in vivo* have a micro-scale granularity, being composed of packed micro-scale cells. We envision that by producing jammed microgel culture media with ECM networks filling the interstitial pore-space, an inanimate tissue-mimicking environment could be developed. We believe that the experiments described here in the simplest formulation of jammed microgel culture medium represent a necessary first-step in following these numerous research directions in soft matter related fields.

Materials and methods

Cell culture

Murine cytotoxic T cells, CTLL-2 (ATCC TIB-214), are cultured in suspension culture flasks and successively passaged before the concentration reached 2×10^5 cells ml^{-1}. To prepare the complete growth medium, RPMI-1640 with L-glutamine media is supplemented with 1 mM sodium pyruvate, 1% penicillin streptomycin solution, 10% FBS and 10% T-STIM with Con-A.

Jammed granular microgel growth medium

To prepare the jammed granular microgel growth medium, we prepare a suspension of carbomer 980 directly in liquid cell growth medium and mixing using a centrifugal speed mixer at 3500 rpm for 15 min. The pH is the adjusted to 7.4 at the incubation condition of 37 °C and 5% CO_2. These jammed microgel samples are maintained at sterile conditions and incubated to culture conditions prior to use.

Cell staining

To track CTLL-2 T cells in 3D jammed microgel growth media, we dispersed fluorescently labeled cells into LLS growth medium at different cell densities. These T cells are fluorescently dyed by treating with 10 μM 5-chloromethyl-fluorescein diacetate (CMFDA) in cell growth medium and 0.2% dimethyl sulfoxide for 30 min. After dyeing, cells are incubated in regular cell growth media for 30 min prior to use.

Cell tracking and analysis

To explore the interaction between cells dispersed in the jammed microgel growth media, we collect time-lapse 3D stacks of T cells on a confocal microscope for 24 h. Individual cell positions are identified using a custom program written in MATLAB. Each cell is then tracked using the algorithm of Crocker and Grier [33]. The average cell displacement is represented here by the mean-square displacement, $\left\langle [\mathbf{r}(t+\tau) - \mathbf{r}(t)]^2 \right\rangle$. Here $\mathbf{r}$ denotes the position of cell at time t, and angle brackets indicate an average over time. These MSDs are computed on a τ-axis with constant spacing. To enable analysis on a logarithmic scale, we re-sample every single-cell MSD on a logarithmic tau-axis, averaging all points that fall within each logarithmically spaced bin. This produces 9 τ's spaced evenly on a logarithmic scale, along with the corresponding averaged MSDs within each bin. This procedure enables performing a discrete logarithmic derivative to solve for alpha without any fitting: $\alpha(\tau) = d[\ln(\mathrm{MSD})]/d[\ln(\tau)]$. To enable a finer bin-spacing and create smoother PDFs that better guide the eye, we revisit the single-cell MSDs, fitting a cubic smoothing spline thorough each MSD, sampling at smaller logarithmically spaced tau intervals. We then, once again, perform a discrete derivative to find $\alpha(\tau)$ in each smaller bin. We manually adjust the smoothness of the spline until the resulting PDFs match the distributions of α found from the case with no fitting. While this procedure produces τ-bins at short times that are not directly measured, matching the splined results to their coarsely sampled counterparts produces the same principle results while creating smoother PDFs.

The various piecewise constant probability density functions described here are produced by creating histograms of measured variables and normalizing. For example, all step-size distribution functions are normalized such that $\sum_j p(d_j)\Delta d_j = 1$, where d_j is the center of the jth step-size bin and Δd_j is the jth bin-width. Normalizing in a way that accounts for changing bin-width is critical when creating PDFs on logarithmic scales. 2D PDFs are normalized in a similar way. For example, the 2D PDF of α and τ is normalized such that $\sum_{j,k} p(\tau_j, \alpha_k)\Delta\tau_j\Delta\alpha_k = 1$. In this case we

J. Phys. D: Appl. Phys. **52** (2019) 024006

T Bhattacharjee and T E Angelini

chose to uniformly sample a in the 2D histogram but logarithmically sample τ.

Imaging

A Nikon Eclipse Ti-E microscope with a C2 confocal scanning system is employed to image cells at 37 °C in 5% CO2. All images processing is done using MATLAB and ImageJ.

Acknowledgments

ORCID iDs

Tapomoy Bhattacharjee https://orcid.org/0000-0001-8899-1379

References

[1] Coussot P *et al* 2009 Macroscopic versus local rheology of yield stress fluids *J. Non-Newton. Fluid Mech.* **158** 85–90

[2] Mattsson J *et al* 2009 Soft colloids make strong glasses *Nature* **462** 83

[3] Fernandez-Nieves A *et al* 2011 *Microgel Suspensions: Fundamentals and Applications* (New York: Wiley)

[4] Tibbitt M W and Anseth K S 2009 Hydrogels as extracellular matrix mimics for 3D cell culture *Biotechnol. Bioeng.* **103** 655–63

[5] Menut P *et al* 2012 Does size matter? Elasticity of compressed suspensions of colloidal-and granular-scale microgels *Soft Matter* **8** 156–64

[6] Pellet C and Cloitre M 2016 The glass and jamming transitions of soft polyelectrolyte microgel suspensions *Soft Matter* **12** 3710–20

[7] Mohan L *et al* 2013 Local mobility and microstructure in periodically sheared soft particle glasses and their connection to macroscopic rheology *J. Rheol.* **57** 1023–46

[8] Romeo G and Ciamarra M P 2013 Elasticity of compressed microgel suspensions *Soft Matter* **9** 5401–6

[9] Seth J R *et al* 2011 A micromechanical model to predict the flow of soft particle glasses *Nat. Mater.* **10** 838–43

[10] Bhattacharjee T *et al* 2018 Polyelectrolyte scaling laws for microgel yielding near jamming *Soft Matter* **14** 1559–70

[11] Saatweber D and Vogt-Birnbrich B 1996 Microgels in organic coatings *Prog. Org. Coat.* **28** 33–41

[12] Saunders B R and Vincent B 1999 Microgel particles as model colloids: theory, properties and applications *Adv. Colloid Interface Sci.* **80** 1–25

[13] Thorne J B, Vine G J and Snowden M J 2011 Microgel applications and commercial considerations *Colloid Polym. Sci.* **289** 625

[14] Timm K *et al* 2011 Particulate lubricants in cosmetic applications *Tribol. Int.* **44** 1695–703

[15] Sonneville-Aubrun O, Simonnet J-T and L'alloret F 2004 Nanoemulsions: a new vehicle for skincare products *Adv. Colloid Interface Sci.* **108** 145–9

[16] Barker P I, Ziskin N A and Grossfeld M J 1982 Multiphase cosmetic composition *Google Patents* US4335103A

[17] Bhattacharjee T *et al* 2015 Writing in the granular gel medium *Sci. Adv.* **1** e1500655

[18] O'Bryan C S *et al* 2017 Three-dimensional printing with sacrificial materials for soft matter manufacturing *MRS Bull.* **42** 571–7

[19] Jin Y *et al* 2016 Granular gel support-enabled extrusion of three-dimensional alginate and cellular structures *Biofabrication* **8** 025016

[20] Bhattacharjee T *et al* 2016 Liquid-like solids support cells in 3D *ACS Biomater. Sci. Eng.* **2** 1787–95

[21] Seliktar D 2012 Designing cell-compatible hydrogels for biomedical applications *Science* **336** 1124–8

[22] Krummel M F, Bartumeus F and Gérard A 2016 T cell migration, search strategies and mechanisms *Nat. Rev. Immunol.* **16** 193

[23] Harris T H *et al* 2012 Generalized Lévy walks and the role of chemokines in migration of effector CD8+ T cells *Nature* **486** 545

[24] Franck C *et al* 2011 Three-dimensional traction force microscopy: a new tool for quantifying cell-matrix interactions *PLoS One* **6** e17833

[25] Steinwachs J *et al* 2015 Three-dimensional force microscopy of cells in biopolymer networks *Nat. Methods* **13** 171

[26] Wolf K *et al* 2003 Amoeboid shape change and contact guidance: T-lymphocyte crawling through fibrillar collagen is independent of matrix remodeling by MMPs and other proteases *Blood* **102** 3262–9

[27] Liétor-Santos J J, Sierra-Martín B and Fernández-Nieves A 2011 Bulk and shear moduli of compressed microgel suspensions *Phys. Rev.* E **84** 060402

[28] Otsu N 1979 A threshold selection method from gray-level histograms *IEEE Trans. Syst. Man Cybern.* **9** 62–6

[29] Mickel W *et al* 2008 Robust pore size analysis of filamentous networks from three-dimensional confocal microscopy *Biophys. J.* **95** 6072–80

[30] Krummel M F, Friedman R S and Jacobelli J 2014 Modes and mechanisms of T cell motility: roles for confinement and Myosin-IIA *Curr. Opin. Cell Biol.* **30** 9–16

[31] Lautscham L A *et al* 2015 Migration in confined 3D environments is determined by a combination of adhesiveness, nuclear volume, contractility, and cell stiffness *Biophys. J.* **109** 900–13

[32] Joyce J A and Fearon D T 2015 T cell exclusion, immune privilege, and the tumor microenvironment *Science* **348** 74–80

[33] Crocker J C and Grier D G 1996 Methods of digital video microscopy for colloidal studies *J. Colloid Interface Sci.* **179** 298–310